ELECTROCHEMICAL AND THEORETICAL EVALUATION OF 4-(4-BROMOPHENYL) THIOSEMICARBAZIDE AS THE CORROSION INHIBITION FOR MILD STEEL IN 1.0 M HCL

Abdelhakim Alrjaibi[1], Emel Bayol[2], and Fatma Kandemirli[3*]

[1] Department of Mechanical Engineering, High Institute of Science and Technology, Zawia Libya

[2] Department of Chemistry, Faculty of Art and Science, Niğde Ömer Halisdemir University, 51240 Niğde, Turkey

[3] Department of Biomedical Engineering, Faculty of Engineering and Architecture, Kastamonu University, 37200 Kastamonu, Turkey

[*] hakimrj2011@yahoo.com

Abstract

This examination researched the impact of changing measures of 4-(4-bromophenyl) Thiosemicarbazide (4-BrPh TSC) by assessing air conditioning impedance and AC and flow potentiometry in a 1.0 M HCl arrangement at 20°C. When the E_{corr} value is -0.518 V, the concentration of the inhibitor solution changes and the grouping of the inhibitor changes. The present's thickness of the anodic and cathodic districts is bring down contrasted with that of the 1.0 M HCl arrangement, with an I_{corr} estimation of 158.78 μA•cm^{-2} in the uninhibited arrangement and 8.10 μA•cm^{-2} at the 1x10^{-2} M concentration of 4-BrPh TSC. The percent restraint proficiency extended from 71% to 95%. For the uninhibited and most astounding grouping of 4-BrPh TSC arrangement, the estimations of R_{pblank} and R_{pinh} were 235 and 2006 Ω.cm^{-2}, separately, CPE_{blank} and CPE_{inh} were 348 and 36 μF.cm^{-2}, individually, n_{blank} and n_{inh} were 0.94 and 0.84. As the R_p esteem builds, the CPE esteem and n diminish as the inhibitor focus increments, potentially because of abatement in neighborhood dielectric steady or an expanded thickness at the metal/arrangement interface. For the subsidiaries of 4-BrPh TSC, the estimation of ΔG^o_{ads} and is -36.00 kJ mol^{-1}, demonstrating that the adsorption of these inhibitors includes two sorts of communications: physical adsorption and chemisorption. The thickness utilitarian hypothesis (DFT) of the B3LYP work with the 6-311G (d,p) premise set was performed .

Keywords: Corrosion; Inhibition; mild steel; Thiosemicarbazide; Quantum chemical studies.

Introduction

A major issue to be dealt with in industries is corrosion, which causes significant burdens as to cost for business. Structures of metallic nature in different industries are in contact with corrosive materials and processes, for which acid solutions are

commonly applied to remove pickling and rust. Materials such as acidification inhibitors are also used to defend against corrosion of metal structures (Obot and Obi-Egbedi, 2010). In this respect, organic inhibitors have appeared to be a safe replacement (Solmaz, 2014). As since the inhibitor can easily form covalent bonds with metal surface (also known as 'chemisorption'), or by means of electrostatic interaction (referred to as 'physical adsorption') between metal surface and inhibitor (Abd El-Nabey et al., 1987; Mahgoub et al., 2010). It has been previously shown that adsorption is primarily dependent on p-electrons, molecular heteroatoms, functional groups and benzene rings to induce inhibitor molecules and more absorbed on the surface of smooth steel. The best effect of organic compounds can be obtained by increasing the electron density of heteroatoms such as sulphur, phosphorus, nitrogen and oxygen also considered as the 'adsorption center (Awad et al., 2000; Doner et al., 2013). In this regard, lately the effectiveness of thiosemicarbazone compounds also as known as organic corrosion inhibitors has been largely that focused on by the research community (Ita and Offiong.,2001; Xu et al,.2014), with reports of the potential of creating complexes with different metals (Casas et al., 2000; Bisceglie et al., 2015).

These compounds owe their increased activity and effectiveness against corrosion to the presence of nitrogen and sulphur, thus generating more inhibition as opposed to compounds with just one of the elements mentioned. Furthermore, compounds with sulphur tend to be more active in general in comparison to oxygen-containing ones with identical structures (Poornima et al., 2011; Karakus and Sayin., 2015). In line with this information, the present work investigates the adsorption and the inhibitory properties of 4-BrPh TSC Figure (1) In the case of dynamic kinetic polarization, the methods such as linear polarization resistance and electrochemical impedance; low carbon steel in 1.0 M HCl solution was pierced. Besides, the density functional theory (DFT) is performed for 4-BrPh TSC.

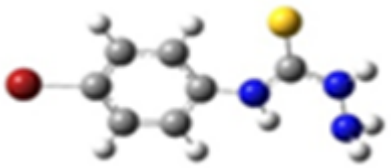

Figure (1): Chemical Structure of 4-BrPh TSC.

Experimental

1. Materials and Test Solutions

Three-electrode battery made of low carbon steel, p assembly was used for testing, the counter electrode was 1 x 1 cm platinum, and Ag / AgCl (3.0 M KCl) was used as the

reference electrode. Low carbon steel (MS) having a mass fraction of 0.11% Si, 1.01% Cr, 0.99% Mn and 97.89% Fe was used for electrochemical measurement purposes. The sample is embedded in the polyester; the surface area of 0.6359 cm^2 is in contact with the corrosive medium, how much corrosive material is present, and the copper wire provides electrical conductivity. Before every attempt, the low carbon steel surface was mechanically polished using different emery papers having different grades. The sample is embedded in the polyester; the surface area of 0.6359 cm^2 is in contact with the corrosive medium, how much corrosive material is present, and the copper wire provides electrical conductivity. Different grades (1000, 600 and 150) of sandpaper, then they are degreased by using acetone, and rinsed with distilled water and placed in a battery. Tests were conducted in 1.0 M HCl solutions with and without of $1x10^{-5}$ – $1x10^{-2}$ M of 4-BrPh TSC.

2. Electrochemical Techniques

Electrochemical experiments were performed by using electrochemical analyser and computer controlled CHI 660B. Before electrochemical measurement, stabilization duration of 1h took place, enough to reach the potential for open circuit corrosion (E_{corr}). Electrochemical tests were done at 293 K. The electrochemical impedance spectroscopy (EIS) experiment was performed under an AC signal with peak-to-peak amplitude of 5 mV at the open circuit potential and a frequency range of 105 Hz to 0.003 Hz. At a scan rate of 0.1 mV s^{-1}, the potential range was evaluated from E_{corr} to be 10 mV, and R_{lp} was measured from the slope of the potential and current. Potentiodynamic polarization measurements were carried out by changing the electrode potential at −300 mV cathodic potential and at +300 mV anodic potential of the corrosion potential versus Ag/AgCl at a scan rate of 2 mV s^{-1}.

3. Quantum Chemical Analysis

Theoretical evaluation was performed on the B3LYP function using density functional theory (DFT) with a 6-311G (d,p) basis set, by using Gaussian program (Gaussian 09 et al.,2009) Other calculations include quantum chemical index, energy of the lowest unoccupied molecular orbital and the highest occupied molecular orbital (HOMO), (LUMO), electronegativity (χ), energy gap (ΔE), softness (σ), hardness (η) chemical potential (μ) and electrophilicity index (ω), Nucleofugality (ΔE_n), and Electrofugality (ΔE_e).

Results and Discussion

1. Potentiodynamic Polarization Measurements

Figure (2) shows the polarization curves of carbon steel electrodes with and without different concentrations of 4-BrPh TSC molecules at 293K. Dynamic potential polarization parameters such as corrosion potential (E_{corr}), corrosion current density

(I_{corr}) and cathode Tafel constant (βc), percentage of inhibition efficiency (IE %) are shown in Table (1). A sample polarization curve is shown in Figure (2).

$$\boldsymbol{\theta = \frac{I^{\circ}_{corr} - I_{corr}}{I^{\circ}_{corr}}} \qquad \textbf{(1)}$$

$$\boldsymbol{IE\% = \theta \times 100} \qquad \textbf{(2)}$$

Although the E_{corr} value was -0.518 V in the uninhibited solution, it moved in the positive direction in a short time as the concentration of the inhibitor increased. As can be clearly seen from Figure (3), the current density of the anode and cathode regions is lower compared to the 1.0 M HCl solution. The i_{corr} and E_{corr} also written differently in low key the change was made accordingly, with a value of 158.78 μA•cm^{-2} in the uninhibited solution and 8.10 μA•cm^{-2} at the 4-BrPh TSC concentration of 1×10^{-2}M.

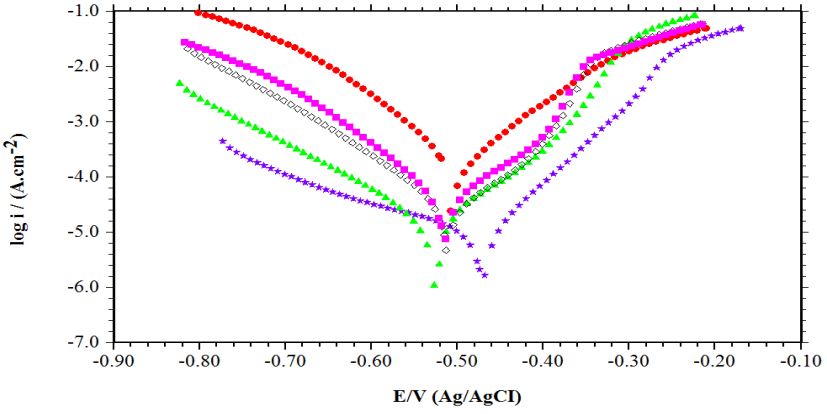

Figure (2): Potentiodynamic Polarization Curves of MS in 1.0 M HCl Solution without (●) and with the Addition of 1x10^{-5} M (■), 1x10^{-4} M (◇), 1x10^{-3} M (▲) and 1x10^{-2} M (★) Different Concentrations of 4-BrPh TSC at 293K.

Table (1): Corrosion Parameters Obtained from Potentiodynamic Polarization Curves for MS in 1.0 M HCl in the Absence and Presence of 4-BrPh TSC in Various Concentrations at 1h.

C(M)	E_{corr} (V/Ag/AgCI)	i_{cor} (μA/cm^2)	- β_c (mV/dec)	IE (%)	θ
Blank	-0.518	158.78	93	-	-
1×10^{-5}	-0.518	46.84	87	71	0.71
1×10^{-4}	-0.515	21.46	98	86	0.86
1×10^{-3}	-0.524	13.38	117	92	0.92
1×10^{-2}	-0.468	8.10	151	95	0.95

With increase in inhibitor concentration, corrosion current densities declined, and also the inhibition efficiency values elevated in all solutions. The percentage inhibition efficiency values varied from 71 % to 95 %.

According to the polarization curve, in the presence of an inhibitor, the curve moves toward the low current density region. When 4-BrPh TSC is added to the acidic solution, both the anode metal dissolution and the cathodic hydrogen evolution reaction are inhibited. The 4-BrP TSC might adsorb and create a covering sheath on the mild steel, thus inhibiting corrosion. As can be seen from Table 1, the maximum displacement of E_{corr} value is about 50 mV. Since the maximum change in E_{corr} value is less than 85 mV, it can be concluded that the inhibitor is a mixed inhibitor. Cathodic Tafel slope (βc) values elevate with the inhibitor. The Tafel slope changes indicate that inhibitors affect hydrogen evolution reaction kinetics, in turn implying elevations in the energy Proton discharge barriers result in reduced gas release. In addition, the polarized cathode branches form a very parallel Tafel line, i.e., the addition of the inhibitor does not change the hydrogen evolution process, and a charge transfer mechanism occurs due to a decrease in surface hydrogen ions of the low temperature steel. In this way, the actual surface area available for H^+ ions is reduced, while the actual reaction mechanism remains unaffected (Aouniti et al. Zhang et al., 2016).

In the anodic field – one has to remember - for potentials higher than -350 mV, a low concentration inhibitor does not alter the current-potential features; yet, in settings containing the highest amounts of an inhibitor, the desorption potential shifts to a more positive potential value defined as ‘desorption potential’. Here, the desorption rate of the inhibitor is greater than its adsorption level, i.e. the type of inhibition of the inhibitor depends on the electrode potential (Liao et al., 2016; Bayol et al., 2007).

2. Electrochemical Impedance Spectroscopy (EIS)

(EIS) is an in situ, non-destructive, fast and applicable method for evaluating metal features covered by organic materials. In addition, there is a wide range of applications for this method to study metal protection by means of organic inhibitors and their characteristics. The approach has offered sound and proven outcomes thanks to low interference with the bilayer at the interface of the metal solution. What’s more, EIS offers an intricate insight into electrochemical system characteristics as well as large amounts of information on kinetic and mechanical properties (Singh et al., 2016; Singh et al., 2016). When analysing impedance data, we applied the view program to model the physical phenomena occurring at the interface of the metal solution. Other circuit models as shown in Figure 3 were used to simulate experimental impedance data for low carbon steel corrosion in corrosive media with and without inhibitors. The representations are as in the following: Rp° = Rct + Rd and Rp =Rct + Rd + Ra + Rf for uninhibited and inhibited solutions. Rs: solution resistance, Rct: charge transfer resistance, Rd: diffusion layer resistance, Ra: resistance of accumulated material at the

metal/solution interface, Rf: membrane resistance, R_{por}: pore resistance, CPE: double layer capacitance and film capacitance, used for Unsuppressed and suppressed solution (Kowsari et al., 2016; Yıldız., 2015). Here, CPE is a constant phase element and n is a phase shift explained as a degree of uniformity surface (Solmaz, 2014; Solmaz, 2010).

$$\mathbf{ZCPE = Y0\text{-}1\ (jw)\text{-}n} \qquad \mathbf{(3)}$$

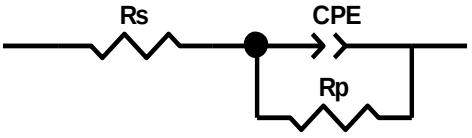

Figure (3): Equivalent Circuit used to fit Impedance Spectra.

In the case where Y0 is a scale factor, j2 = -1 is a hypothesis number, w is the angular frequency in rad-1 ($w = 2\pi f_{max}$, f_{max} is the frequency at which the imaginary part of the impedance is the largest). The inhibition efficiency percentage (IE %) Is determined using the following expression (Solmaz, 2010).

$$\boldsymbol{\theta} = \frac{\boldsymbol{R_P - R_p^0}}{\boldsymbol{R_P}} \qquad \mathbf{(4)}$$

$$\boldsymbol{IE\% = \theta \times 100} \qquad \mathbf{(5)}$$

Where R_p and $R°_p$ are the polarization resistances of the electrodes with and without inhibitor respectively. Table (2) shows the corresponding corrosion parameters obtained from Nyquist curves for MS in 1.0 M HCl and Figure (4) depicts impedance plot (a) N_{yquist}, (b) Bode modulu and (c) phase angle representation.

Table (2): Corrosion Parameters Obtained for MS in 1.0 M HCl in the Absence and Presence of 4-BrPh TSC at 293K.

C(M)	E_{corr} (V)	R_s ($\Omega.cm^{-2}$)	R_p ($\Omega.cm^{-2}$)	CPE		IE (%)	R_{lp}	IE (%)
				($\mu F.cm^{-2}$)	(n)			
1.0 M HCl	-0.520	2	110	348	0.94	-	102	
1×10^{-5}	-0.516	1.1	235	278	0.89	53	454	77
1×10^{-4}	-0.513	1.7	656	68	0.90	83	795	87
1×10^{-3}	-0.511	1.8	1122	42	0.87	90	1272	92
1×10^{-2}	-0.471	2.7	2006	36	0.84	95	2119	95

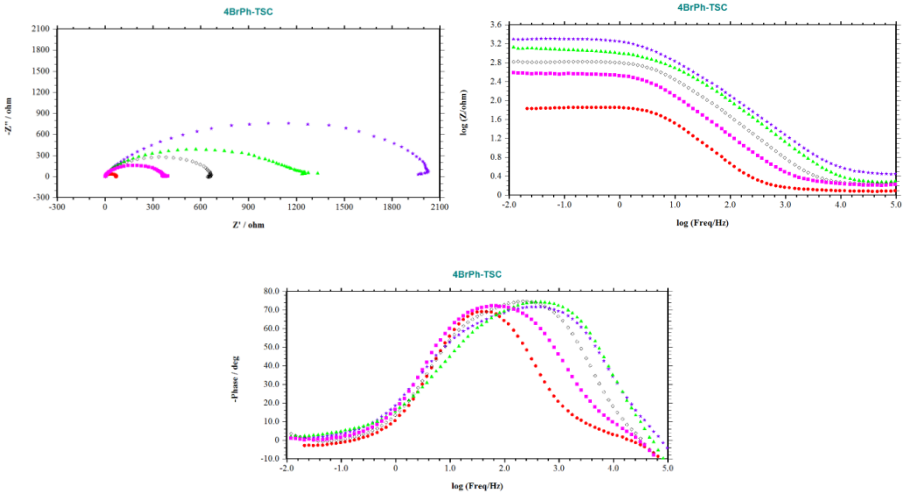

Figure (4): Nyquist Curves of MS in 1,0 M HCl Solution without (●) and with the Addition of 1x10^{-5} M (■), 1x10^{-4} M (◇), 1x10^{-3} M (▲) and 1x10^{-2} M (★) Different Concentrations of 4-BrPh TSC.

As the theory of electrochemical impedance spectroscopy suggests, low carbon steel often does not produce a complete semicircle. This difference from the ideal semicircular shape is usually explained by the surface dispersion, impurities, dislocations, grain boundaries, adsorption of the inhibitor, formation of the porous layer, and frequency dispersion caused by uniformity on the surface of the electrode. According to Table (2), the values of R_{pblank} and R_{pinh} are 235 and 2006 Ω.cm^{-2}, respectively, and the values of CPE_{blank} and CPE_{inh} are 348 and 36 µF.cm^{-2}, respectively, and the values of n_{blank} and n_{inh} are 0.94 and 0.84, which are unsuppressed. The highest concentration is the 4-BrPh TSC solution. As the R_p values rise, The CPE value and n decrease with increasing inhibitor concentration, which may be due to a decrease in local dielectric constant or an increase in thickness of the metal solution interface. The maximum concentration of linear polarization resistance (R_p) values based on the blank LPR method and 4-BrPh TSC showed an increase from 102 to 2119. Table (2). The correlation between EIS and LPR results is at an acceptable level.

3. Adsorption Isotherm

These define the interaction that the inhibitor and MS surface have. The adsorption of inhibitor molecules on the metal surface is a in a way a replacement phenomenon where water molecules taken in change places with organic molecules. The experimental data yielded is fitted to numerous adsorption isotherms, whose Langmuir isotherm proved to offer the best fit. The Langmuir isotherm is a plot of C vs. C/Θ as appears in Eq. (6), (Solmaz, 2014).

$$C/\Theta = 1/K_{ads} + C \qquad (6)$$

Where K_{ads} is the equilibrium constant of adsorption, C is the concentration of the inhibitor, and Θ is the surface coverage. Further, the standard free energy of adsorption ($\Delta G°_{ads}$) can be computed from Eq- (7), (Solmaz, 2014).

$$K_{ads} = \frac{1}{55,5}\exp\left(-\frac{\Delta G^{\circ}_{ads}}{RT}\right) \qquad \textbf{(7)}$$

The Langmuir adsorption isotherms of 4-BrPh TSC is shown in Figure (5).

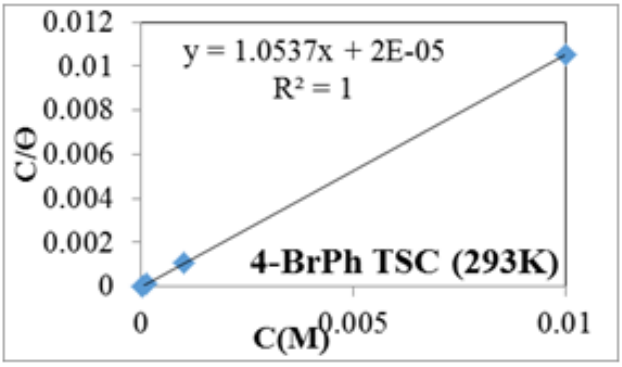

Figure (5) Langmuir Adsorption of 4-BrPh TSC on the Mild Steel Surface in 1.0 M HCl Solution.

The values of K_{ads} 50000 and negative Gibbs free energy of adsorption 36.00 kj mol^{-1} are obtained from Eq. (6) and Eq. (7), respectively. The high K_{ads} for the 4-BrPh TSC implies higher adsorption on MS surfaces in 1.0 M HCl solution at 293 K. The value of the standard free energy of adsorption represents the simultaneous adsorption of the molecule on the surface of MS and the high interaction between the inhibitor molecule and the MS. Typically, the standard value of free energy of -20 kJ mol^{-1} or less is related to the electrostatic interaction between charged molecules and charged metal surfaces (also known as "physical adsorption"). Those from a negative value of -40 kJ mol^{-1} or more include loading or transferring an inhibitor molecule to a metal surface to form a coordinate covalent bond (or "chemisorption") (Olasunkanmi et al., 2016; Palanisamy et al., 2017). In our measurements, for 4-BrPh TSC, the value of $-\Delta G^{\circ}_{ads}$ was 36.00 kJ mol^{-1}, thus indicating that adsorption of these inhibitors requires two types of interactions: chemisorption and physical adsorption (Olasunkanmi et al., 2016; Palanisamy et al., 2017).

Computational Details

1. Quantum Chemical Calculations

$$x = -\mu = -\left(\partial\mu/\partial N\right)_{v(r)} \quad (8)$$

$$\eta = \frac{1}{2}\left(\partial\mu/\partial N\right)_{v(r)} = \frac{1}{2}\left(\frac{\partial^2\mu}{\partial N^2}\right)_{v(r)} \quad (9)$$

Pearson and Parr came up with a mathematical expression for the reactivity descriptors mentioned earlier in accordance ionization energy and electronic affinity values of the compounds using a finite difference approximation (Parr et al., 1999). Eqs (8) and (9) these formulas obtained are given as:

$$\eta = \frac{1-A}{2} \quad (10)$$

$$x = -\mu = \frac{1+A}{2} \quad (11)$$

Based on the theory, the negative values of the most occupied and least empty molecular orbital energy, in turn, account for ionization energy and electron affinity ($-E_{HOMO}$ = I and $-E_{LUMO}$ = A). Henceforth, factors such as chemical hardness, chemical potential and electronegativity are measured with the formula below and in theoretical terms (Islam and Ghosh., 2011).

$$\mu = -x = \frac{E_{LUMO}+E_{HOMO}}{2} \quad (12)$$

$$\eta = \frac{E_{LUMO}+E_{HOMO}}{2} \quad (13)$$

R.G. Pearson, in this regard, suggests that softness is the multiplicative reciprocal of hardness (Pearson., 1963).

$$\sigma = \frac{1}{\eta} = \frac{2}{E_{LUMO}-E_{HOMO}} \quad (14)$$

Electrophilicity can serve as a reactive descriptor to be applied to compare electron-donating ability in molecules (Chattaraj and Roy., 2007). Lately, Parr suggested an electrophilicity index, which has been commonly utilized in numerous works related to site selectivity, toxicity and corrosion as inhibitors of molecule performance. This index is elaborated with mathematical formulas. Also, it has to be kept in mind that Parr is expressed as the reciprocal multiplicative reciprocal of nucleophilicity (Parr and Chattaraj, 1991).

$$\omega = \frac{\mu^2}{2\eta} = \frac{x^2}{2\eta} \quad (15)$$

$$\varepsilon = {}^{1}/_{\omega} \qquad \textbf{(16)}$$

According to Figure (6), the combined form of inhibitor molecules, the HOMO location, is primarily dispersed over the S atom from the thiosemicarbize group; whereas the LUMO location is distributed on all molecules, thus indicating that electrons are transferred from the orbital of S to the metal and that those electrons in the occupied orbital of metal are moved to the LUMO benzene ring and the S atom. The frontier orbital energies calculated with B3LYP/6-3G (d,p) are shown in Figure (7) under four conditions: neutral and gaseous phase neutral forms, and gas phase and aqueous phase protonated forms. In all the cases, the calculated (E_{HOMO}) values for the B3LYP/6-311g(d, p) baseline set for 4-BrPh TSC molecules were -5.974 eV, -6.257 eV, -9.642 eV, and -6.807 eV, respectively. Also, 4-BrPh TSC, 4- BrPh TSC-w, 4-BrPh TSC-p and 4-BrPh TSC-p-w were observed in the molecule.

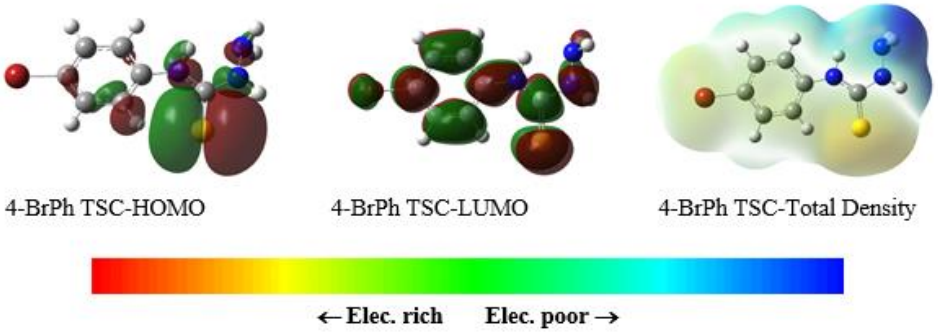

Figure (6): The Optimized Molecular Structure, HOMO, LUMO and Total Density of 4-BrPh TSC.

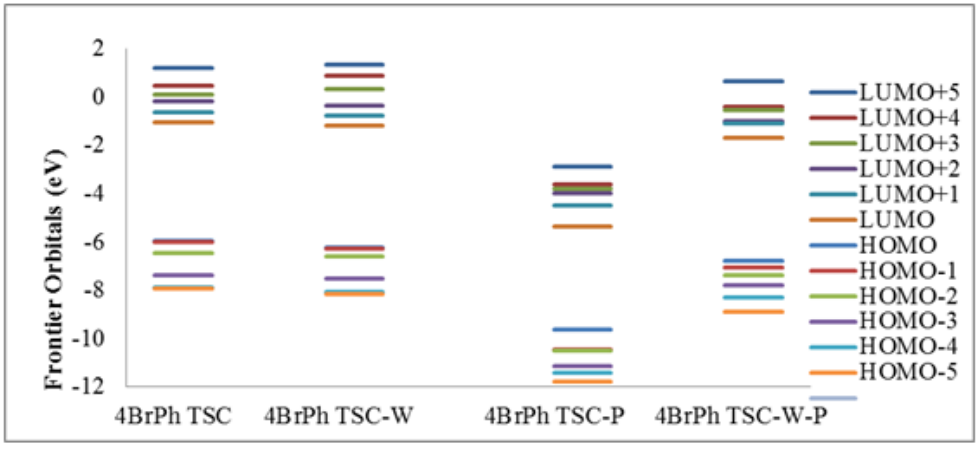

Figure (7): The Calculated HOMO, LUMO and Energy Gap Parameters for Compound in the Neutral and Water Forms in Gas Phase and Pronated Phase by using B3LYP/6-311G(d,p) Basis Set.

The E_{LUMO} values of these molecules are calculated with B3LYP/6-1G (d,p) basis set for the 4-BrPh TSC molecules in four situations as -1.041 eV, -1.177 eV, -5.369 eV and -1.702 eV. These results have also been reached in the molecules 4-BrPh TSC, 4-BrPh TSC-w, 4-BrPh TSC-p and 4-BrPh TSC-pw, respectively.

Table (3): The Calculated Parameters by B3LYP/6-311G (d, p) of Molecules Under Study for Neutral and Protonated Form in Gas and Water Phase.

Compounds	HOMO (eV)	LUMO (eV)	ΔE (eV)	η(eV)	σ(eV)	X(eV)	μ(eV)	ω(eV)	$\Delta E_{n,}$ (eV)	$\Delta E_{n,}$ (eV)
4-BrPh TSC	-5.974	-1.041	4.933	2.467	0.203	3.507	-3.507	2.494	0.220	7.234
4-BrPh TSC-w	-6.257	-1.177	5.080	2.540	0.197	3.717	-3.717	2.720	0.273	7.707
4-BrPh TSC-p	-9.642	-5.369	4.274	2.137	0.234	7.506	-7.506	13.182	6.745	21.756
4-BrPh TSC-wp	-6.807	-1.702	5.105	2.553	0.196	4.254	-4.254	3.545	0.567	9.076

The frontier orbital energies calculated with B3LYP/6-3++G (2d, 2p) are shown in Table (4) under four conditions: neutral forms and protonated forms in gas phase and aqueous phase. In all four cases, the calculated E_{HOMO} values for the B3LYP/6-311++G (2d, 2p) basis set for 4-BrPh TSC molecules were -6.033 eV, -6.293 eV, -9.649 eV, and -6.812 eV, respectively. The E_{LUMO} of these molecules values calculated with B3LYP/6-311++G(2d,2p) basis set for 4-BrPh TSC molecules in four situations (neutral forms and protonated forms in gas phase and aqueous phase) were 1.210 eV, - 1.265 eV, -2.383 eV and -5.527 eV respectively. The E_{HOMO} increases are as follows 4-BrPh TSC > 4-BrPh TSC-w > 4-BrPh TSC-w-p > 4-BrPh TSC-p. As seen in Table (4), the values are -6.033 eV, -6.293 eV, -6.812 eV, -9.649 eV, respectively.

Table (4): The Calculated Parameters by B3LYP/6-311++G (2d,2p) of Molecules Under Study for Neutral and Protonated Form in Gas and Water Phase.

Compounds	HOMO (eV)	LUMO (eV)	ΔE	H	σ	X	μ	ω	$\Delta E_{n,}$	$\Delta E_{n,}$
4-BrPh TSC	-6.033	-1.210	4.823	2.411	0.207	3.622	-3.622	2.720	0.304	7.547
4-BrPh TSC-w	-6.293	-1.265	5.029	2.514	0.199	3.779	-3.779	2.840	0.318	7.876
4-BrPh TSC-p	-9.649	-5.527	4.122	2.061	0.243	7.588	-7.588	13.968	7.411	22.587
4-BrPh TSC-w-p	-6.812	-2.383	4.430	2.215	0.226	4.597	-4.597	4.772	1.282	10.476

For the E_{LUMO} increases in 4-BrPh TSC > 4-BrPh TSC-w > 4-BrPh TSC-w-p > 4-BrPh TSC-p, the values are -1.210 eV, -1.265 eV, -2.383 eV, and -5.527 eV, respectively.

The energy gap increases for 4-BrPh TSC-p > 4-BrPh TSC-w-p > 4-BrPh TSC > 4-BrPh TSC-w, the values are 4.122 eV, 4.430 eV, 4.823 eV, and 5.029 eV, respectively.

Conclusion

Adsorption in inhibitors used on the surface of mild steel revealed with the Langmuir isotherm takes place with both in physical and chemical form. With added inhibitor concentration, corrosion current densities dropped while inhibition efficiency values elevated. Tafel polarization revealed a combined form of inhibition pattern in the corrosion inhibitor under study. In addition, our EIS study shows that as polarization resistance becomes more, the CPE and n values decline and concentration increases because of reduction in the local. The dielectric constant and/or the additional thickness of the metal/solution interface. The value of ΔG° ads is -46.00 kJ mol^{-1} of 4-BrPh TSC, which means that the adsorption of these inhibitors occurs in two ways: chemisorption and physical adsorption. Quantum chemistry studies complement the experimentally observed order of inhibition efficiency. Based on E_{HOMO} and E_{LUMO} values, natural species substances Materials are more likely to interact with the metal surface. In the same way, the ΔE values imply that protonated species have more tendencies toward interaction with the metal surface.

References

- I.B Obot, N.O. Obi-Egbedi (2010). Corros. Sci., 52 -198.
- R. Solmaz, (2014). Corros. Sci., 79 -169.
- B.A. Abd El-Nabey, M. El-Gamal, E. Khamis, F. Mahgoub (1987). Surf. Coat. Technol., 31- 89.
- F.M. Mahgoub, B.A. Abdel-Nabey, Y.A. El-Samadisy (2010). Mater. Chem. Phys., 120 - 104.
- M.K. Awad., F.M. Mahgoub, M.M. El-Iskandarani (2000). J. Mol. Struct. Theochem., 531-105.
- Doner, E.A. Sahin, G. Kardas, O. Serindag, Corros. Sci., 66 - 278.
- B.I. Ita, O.E. Offiong. Mater (2001). Chem. Phys.,70 - 330.
- Xu, W. Yang, Y. Liu, X. Yin, W. Gong, Y. (2014). Chen, Corros. Sci., 78 - 260.
- J.S. Casas, M.S. García-Tasende, J. Sordo. Coord. (2000). Chem. Rev., 209 -197.
- F. Bisceglie, G.D. Monte, P. Tarasconi, G. Pelosi (2015). Inorg. Chim. Acta, 434 -

143.

- T. Poornima, J. Nayak, A.N. Shetty (2011). Corros. Sci., 53 - 3688.
- N. Karakus, K. Sayin (2015). J. Taiwan Inst. Chem. Eng., 48 - 95.
- Gaussian 09, Revision, A. "1, MJ Frisch, GW Trucks, HB Schlegel, GE Scuseria, MA Robb, JR Cheeseman, G. Scalmani, V. Barone, B. Mennucci, GA Petersson et al., Gaussian." Inc., Walling ford CT (2009). 121 - 150.
- Aouniti, H. Elmsellem, S. Tighadouini, M. Elazzouzi, S. Radi, A. Chetouani, A. Zarrouk (2016). J. Taibah Univ. Sci., 10 - 774.
- R. Ma. Zhang, H. Liu, Y. Liu, S. Li, L. Niu (2016). J. Mol. Liq., 222 - 671.
- L.L. Liao, S. Mo, J.L. Lei, Q.H. Luo, B.N. Li (2016). J. Colloid Interface Sci., 474 - 68.
- E. Bayol, K. Kayakırılmaz, M. Erbil (2007). Mater. Chem. Phys., 104 - 74.
- P. Singh, V. Srivastava, M.A. Quraishi (2016). J. Mol. Liq., 216 - 164.
- D.K. Singh, S. Kumar, G. Udayabhanu, P.R. John (2016). J. Mol. Liq., 216 - 738.
- E. Kowsari, Y.S .Arman, H.M. Shahini, H. Zandi, A. Ehsani, R. Naderi, M. Mehdipour (2016) Corros.Sci., 112 - 73.
- R. Yıldız (2015). Corros. Sci., 90 - 544.
- R. Solmaz (2014). Corros. Sci., 79 - 169.
- R. Solmaz (2010). Corros. Sci., 52 - 3321.
- R. Solmaz (2014). Corros. Sci., 79 - 169.
- O.L. Olasunkanmi, M.M. Kabanda, E.E. Ebenso (2016). Physica E., 76 - 109.
- K. Palanisamy, P. Kannan, A. Sekar (2017). Egypt. J. Pet., in press.
- R. G. Parr, L. V. Szentpaly, S. Liu (1999). J. Am. Chem. Soc., 121 - 1922.
- N. Islam, D. Chandra Ghosh (2011). Molecular Physics, 109 - 917.
- G.R. Pearson (1963). J. Am. Chem. Soc., 85 - 3533.

- K.P. Chattaraj, R.D. Roy (2007). Chem. Rev., 107 - PR46.
- G.R. Parr, K.P. Chattaraj (1991). J. Am. Chem. Soc., 113 - 1854.